

Article

Using 3-Isocyanatopropyltrimethoxysilane to Decorate Graphene Oxide with Nano-Titanium Dioxide for Enhancing the Anti-Corrosion Properties of Epoxy Coating

Weihang Li, Bojun Song, Shirui Zhang, Fan Zhang, Chang Liu, Nan Zhang, Huiling Yao and Yuanchang Shi *

Key Laboratory for Liquid-Solid Structural Evolution and Processing of Materials (Ministry of Education), Shandong University, Jingshi Road 17923, Jinan 250061, China; jnwh19990909@163.com (W.L.); bj19941021@163.com (B.S.); 17853143187@163.com (S.Z.); zhangfan1176@163.com (F.Z.); LiuChang981021@163.com (C.L.); endiling@126.com (N.Z.); yaohuiling1982@126.com (H.Y.)

* Correspondence: yuanchangshi@sdu.edu.cn; Tel./Fax: +86-0531-88392616

Received: 7 March 2020; Accepted: 2 April 2020; Published: 6 April 2020



Abstract: In this paper, the graphene oxide loaded with nano titanium dioxide ($\text{TiO}_2\text{-GO}$) was synthesized through 3-isocyanatopropyltrimethoxysilane (IPTMS) and characterized by Fourier transform infrared spectroscopy (FTIR), X-ray diffraction analysis (XRD), X-ray photoelectron spectroscopy (XPS), scanning electron microscopy (SEM), thermogravimetric analysis (TGA), and dispersion test. The results illustrated our modification was successful and $\text{TiO}_2\text{-GO}$ was transferred from hydrophilic to hydrophobic. That greatly enhanced the dispersity of $\text{TiO}_2\text{-GO}$ in epoxy through the observation of the coating morphology test. Moreover, the impact of $\text{TiO}_2\text{-GO}$ on anti-corrosion property in epoxy was investigated by Electrochemical Impedance Spectroscopy (EIS). Comparing to pristine particles including GO and TiO_2 , $\text{TiO}_2\text{-GO}$ could more significantly improve the resistance of corrosion with the help of IPTMS. Furthermore, the anti-corrosion mechanism of $\text{TiO}_2\text{-GO}$ in epoxy was tentatively proposed and discussed.

Keywords: graphene oxide; titanium dioxide; 3-isocyanatopropyltrimethoxysilane; epoxy; modification; anti-corrosion

1. Introduction

Corrosion, as an unavoidable problem, occurs in the process of metal application, roughly leading to the direct and indirect economic loss of several hundred billion every year [1]. In reaction to this phenomenon, protective coatings are often conducted on the metal substrates to cut the loss as much as possible. Because of the unique advantages, including the low shrinkage rate, the relatively low cost, the high bonding strength, and the outstanding corrosion resistance, etc [2–4], epoxy becomes one of the most frequently used coatings among the organic coatings. However, epoxy also has its own flaws that limit its further application like high brittleness, low tenacity and thermal shock resistance, and poor friction and wear properties [5]. Moreover, another issue is that the film would generate micro-pores with the solvent evaporating during the solidification. That would result in the more severe penetration of all gases and salts such as O_2 , H_2O , and Cl^- [6,7]. To overcome this shortcoming, inorganic fillers like carbon black, clay, and silica were often added to the films, especially in practical use [8–10]. According to Liu et al., with the doping of the functional talcum powder, the corrosion performance of the resin enhanced enormously [11]. Ahmed et al. [12] prepared core-shell ferrites/kaolin pigments that combine the properties of both and exhibit better corrosion protection properties. While, recently,

some experts attempted to incorporate the nano-scale fillers to the coating and found that it could enhance the property of coating more effectively [13–15]. Palraj et al. [16] compared and evaluated the performance of nano-silica and micro-silica epoxy composite coatings with the methods of salt spray test and EIS test, whose experimental results reflected that epoxy with nano-silica had better barrier properties. Ramezanzadeh and Attar [17] explored the size effect of ZnO particles on the corrosion resistance behavior in epoxy-polyamide coating. It was found that nano-scale ZnO could make more contribution to improving the anti-corrosion performance than the micro sized pigments.

Graphene oxide (GO), as a new century 2D nanomaterial, has attracted much attention in the last few years [18]. Due to the exceptional capabilities of great electrical [19] and thermal conductivity [20], high rigidity [21], high specific surface area, and optical transparency [22], GO has been widely explored for the applications in sensors [23], catalysis [24], energy conversion and storage [25], etc. In respect of coating, GO is an excellent filler, for it could improve not only the mechanical but also antiseptic properties [26–28]. However, based on GO's characteristics of natural agglomeration and the difference of the applicable system, there is a problem of compatibility between organic matrix and GO. Therefore, GO usually needs to be modified before using since the properties of composites depend heavily on the dispersion of GO in the system and the interface interaction between them. One of the most common approaches is to grafting other nano hydrophobic particles on it. The advantage of this method is that it could increase the layer spacing, making GO turn into the loose state as well as preserve the properties of GO [29,30]. Furthermore, the grafted nano-particle would also enhance the coating performance because of its characteristics. There are many nano-particles suitable for decoration, such as SiO_2 , ZnO, Al_2O_3 , and TiO_2 . Many experts have done a lot of related researches, while only a few are associated with GO decorated by nano-titanium dioxide (nano- TiO_2). However, according to the existing results, nano- TiO_2 was proved to have a positive impact on corrosion resistance of organic coatings [14,31,32].

Therefore, in this paper, we put forward a new approach to modify GO with nano- TiO_2 by 3-isocyanatopropyltrimethoxysilane (IPTMS), and the composition, structure, and morphology of TiO_2 -GO were characterized. The TiO_2 -GO nanocomposites were synthesized, utilizing IPTMS in this work. The specific reaction process is shown in Figure 1. Isocyanate group-terminated ($-\text{N}=\text{C}=\text{O}$), on the one side of IPTMS, reacted with hydroxyl ($-\text{OH}$) and carboxyl ($-\text{COOH}$) of GO. The methoxy group ($-\text{OCH}_3$), on the other side, conjugated to the nano- TiO_2 via the dehydration condensation reaction. Considering the high reactivity of IPTMS, our method is much easier to realize, and it helps to improve the reaction efficiency. In addition, the GO, nano- TiO_2 , and TiO_2 -GO nanocomposites were added into epoxy, respectively, with a low weight loading. Then, the corrosion resistance behavior and dispersion performance of all the films were tested and compared.

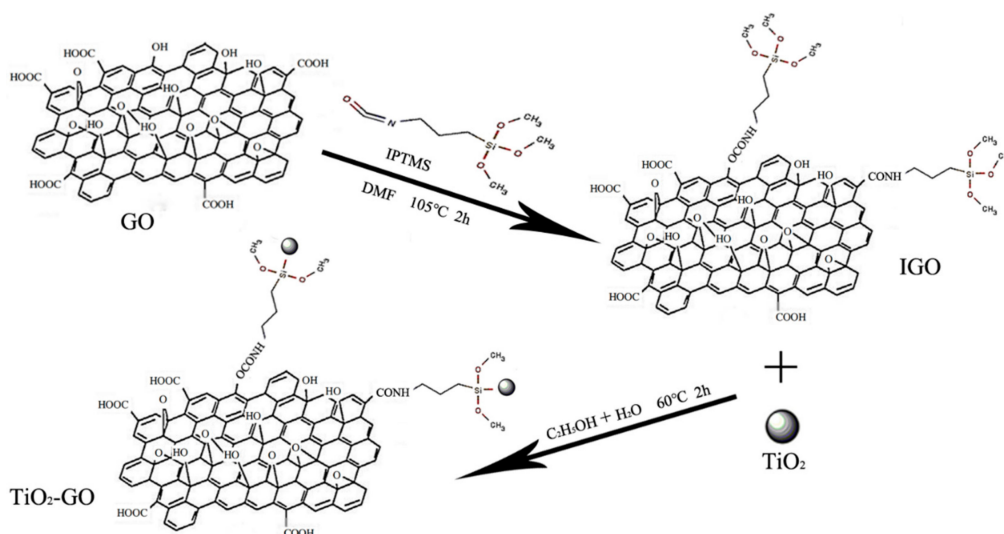


Figure 1. The mechanism of modification of graphene oxide (GO).

2. Experimental

2.1. Materials

The natural graphite powder (325 mesh) was provided from Beijing Jinglong special carbon graphene factory (Beijing, China). The epoxy resin and polyamide hardener (E44/651) were obtained from Phoenix Coatings Co., Ltd. (Wuxi, China). The nano-TiO₂ and IPTMS were supplied by Shanghai Aladdin Biochemical Technology Co., Ltd. (Shanghai, China). The additives of coating (dispersant-2152, defoamer-085, leveling agent-320) were obtained from BYK-Chemie GmbH (Wesel, Germany). Ethanol (C₂H₅OH), acetone (CH₃COCH₃), butyl alcohol, xylene, N, N-dimethylformamide (DMF), sodium nitrate (NaNO₃), 37% hydrochloric acid (HCl), 30% hydrogen peroxide (H₂O₂), 98% sulfuric acid (H₂SO₄), and potassium permanganate (KMnO₄) were all purchased from Chinese medicine group chemical reagent co., Ltd. (Shanghai, China). The deionized water (DI) was self-made in the laboratory. All the reactants were used with no further purification.

2.2. Preparation of TiO₂-GO Nanocomposites

GO was synthesized by the Hummers method [33,34], and the preparation process of TiO₂-GO nanocomposites went through two separate steps. The first step was preparing functionalized GO (F-GO) with the help of IPTMS. Another step was synthesizing TiO₂-GO nanocomposites that decorating F-GO with nano-TiO₂. The specific procedures were as follows:

Firstly, 0.1 g GO was added in 50 mL DMF and sonicated for 20 min to be a homogeneous state. Then 1 g IPTMS was dropped in the solution under stirring at 105 °C for 2 h. Subsequently, the suspension was centrifuged and washed with anhydrous ethanol three times to remove the residual IPTMS and DMF to obtain F-GO.

Next, the F-GO was dispersed in 25 mL ethanol and 0.03 g nano-TiO₂ was dissolved in 25 mL DI both by ultrasound for 20 min. Subsequently, the nano-TiO₂ was slowly dropped in the F-GO ethanol solution under rapid stirring at 60 °C for another 2 h. After that, the mixture was centrifuged and washed with DI and anhydrous ethanol three times, respectively. Lastly, the resultant product was dried at 55 °C for 24 h in the oven.

2.3. Preparation of TiO₂-GO/Pure Epoxy (EP) Coating

In our experiment, firstly, 0.1 wt.% TiO₂-GO, GO, and nano-TiO₂ were separately dispersed in 10 g solvent under sonicating for 20 min. The solvent is the mixture of butyl alcohol and xylene in the ratio of 3:7 wt. Then 30 g epoxy was mixed in the suspension, using a glass rod to stir it until the resin dissolved in the solvent. Next, adding corresponding quantity hardener and coating additives (dispersant-2152, defoamer-085, leveling agent-320), the quantity ratio of resin and hardener is 3:1, kept stirring to let resin and hardener mix homogeneously. Making the bubbles rise out of the surface by setting down for 10 min, the TiO₂-GO/EP coating was finished.

Finally, the prepared coating would be applied on the treated tinfoil panels with a dimension of 120 by 50 by 0.28 mm. Then before brushing, the panels were all abraded by 400, 800, and 1200 grades of sandpapers and washed by DI and acetone to remove oil and impurities. For the performance comparison, four sets of samples were conducted and cured at room temperatures for 120 h; they are pure EP, GO/EP, TiO₂/EP, and TiO₂-GO/EP. The final thickness of the coating layer was about 100 ± 5 μm for the corrosion test.

2.4. Characterization

2.4.1. TiO₂-GO Nano-Particles Characterizations

Spectroscopy analyses of the TiO₂-GO nano-particles were measured by FT-IR and XPS. The FT-IR spectrums were recorded by using a Bruker Vector-22 infrared spectrometer (Bruker, Karlsruhe, Germany) over the wave number range of 400–4000 cm⁻¹. The testing samples were prepared through

the potassium bromide pellet method. To determine the composition, XPS experiments were employed by using a Thermo Scientific Escalab 250Xi spectrometer (Escalab, Gillingham, UK) that equipped with Al K_{α} X-ray source. The shift of binding energy was calibrated which was based on the C1s peak (285 eV). The phase crystal structures of GO, nano-TiO₂, and TiO₂-GO were examined by X-ray diffraction analysis via using Bruker D8 Advance (Bruker, Karlsruhe, Germany). The diffraction pattern was collected at a scan rate of 5°/min in the range of 5–90°. The morphology of GO and TiO₂-GO were obtained through scanning electron microscopy (SEM). By using SEM JEOL-6701F (JEOL, Saitama, Japan), the microstructure of nano-particles was observed. Thermo-gravimetric analysis (TGA) of the particles was tested by model Mettler Toledo (Mettler Toledo, Manchester, UK) with a heating rate of 10 °C/min under nitrogen atmosphere, the temperature region is from 30 to 700 °C. The dispersion tests were also carried out to examine whether the nano-particles was hydrophilic or hydrophobic. In that section, 15 mg GO and TiO₂-GO were added into 15 mL water and ethanol in a sample bottle separately, four samples were sonicated for 20 min, observed, and recorded the phenomenon after setting 1 h and 3 h, respectively.

2.4.2. Test of TiO₂-GO /EP Coatings

Two kinds of tests were carried out in this section. One was to observe the state of TiO₂-GO in EP by SEM. The other was to investigate and compare the anti-corrosion property of four samples via the EIS test by using Zahner_IM6e (Zahner, Saxony, Germany). The test system consisted of a three-electrode cell including a saturated calomel electrode, a platinum electrode, and a coated tinplate were used as reference, counter and working electrodes. The measure of the working electrode area that revealed to 3.5% NaCl solution was 3.799 cm². Our measurements were recorded after immersing for 1 h and 120 h, respectively. The amplitude sinusoidal voltage in test was set as 10 mV with the frequency range from 10⁻² Hz to 10⁵ Hz.

3. Results and Discussion

3.1. FT-IR Spectroscopy

FT-IR test was performed to investigate the functional group of GO and TiO₂-GO particles. The FT-IR spectra of the samples is shown in Figure 2. For GO, the characteristic absorption peaks at 3420 cm⁻¹ nearby indicate the hydroxyl groups. The rest peaks of GO include C–O vibrations of epoxide at 1047 cm⁻¹, C=O and O–H vibrations of carboxyl groups at 1710 and 1384 cm⁻¹, and C=C skeletal vibrations at 1630 cm⁻¹ [28,35]. Regarding the spectra of TiO₂-GO, it not only remains all characteristic absorption peaks of GO but also owns its particular peaks from IPTMS including the –NH and C–N stretching vibration of secondary amines at 3165 and 1259 cm⁻¹, symmetric and asymmetric stretching vibrations of –CH₃ and –CH₂ groups at 2971 and 2921 cm⁻¹ [36–38]. In addition, a broad and intense peak from nano-TiO₂ that represents Ti–O–Ti could be seen at the low wavenumber region. At 1054 cm⁻¹ nearby, the C–O vibrations peak becomes more intense and sharper, that is attributed to the overlap with the bending vibration of C–O–Si peak [39]. According to that peak, it could be concluded that GO has reacted with IPTMS molecules and the reaction products contains Ti–O–Ti bonds.

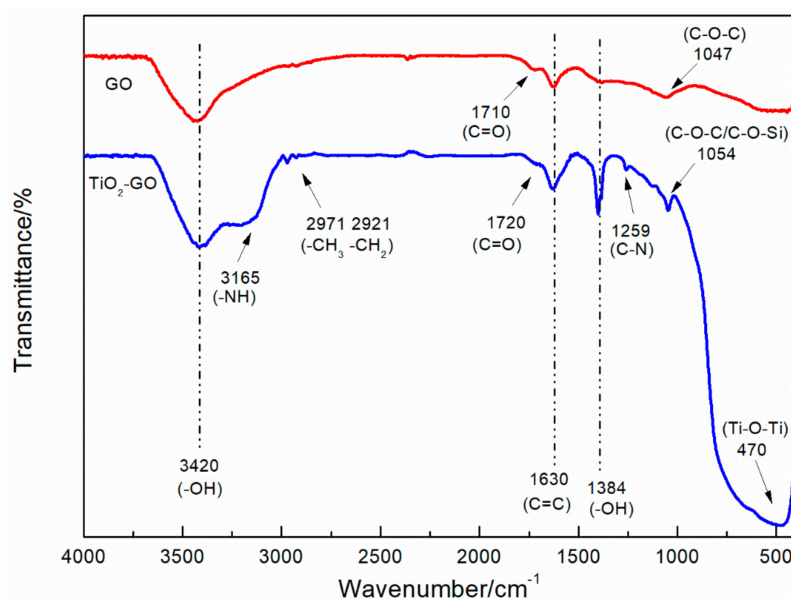


Figure 2. FT-IR spectra of TiO₂-GO and GO.

3.2. XRD Analysis

The XRD patterns which are about GO, nano-TiO₂, and TiO₂-GO are presented in Figure 3. It could be observed that TiO₂-GO possesses both the characteristic diffraction peaks of GO and nano-TiO₂, and the corresponding peaks are observed at 9.84° for GO and 7.90° for TiO₂-GO. According to Bragg’s law:

$$n\lambda = 2d\sin\theta \tag{1}$$

the D-spacing of our particles could be obtained by calculating. Therefore, there is an increment of D-spacing from 8.96 Å to 10.94 Å. That may attribute to the process of decoration; the closely-stacked structure of GO turns to be loosened during the reaction. On the other hand, this indicates the impact of nano-TiO₂ on the GO.

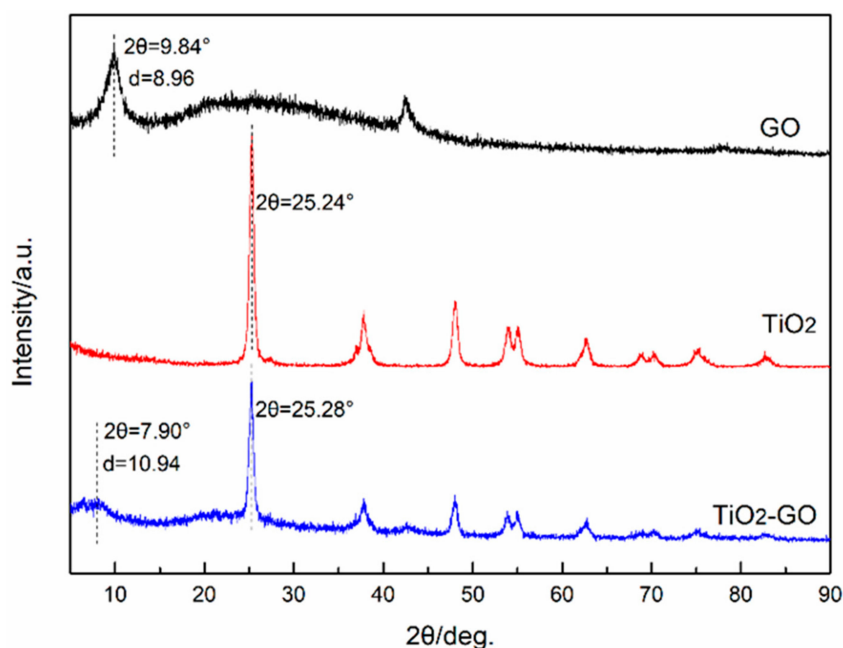


Figure 3. XRD patterns of GO, nano-TiO₂, and TiO₂-GO.

3.3. XPS Analysis

XPS test was performed to examine the exact element that composed of $\text{TiO}_2\text{-GO}$ as well as the chemical bonds [40]. The more detailed information is exhibited in Figure 4. The XPS spectrum indicates that the corresponding peaks including C 1s, O 1s, Ti 2p, N 1s, Si 2s, and Si 2p suggest $\text{TiO}_2\text{-GO}$ is composed of these elements. According to the high resolution spectra, the C 1s are decomposed into several peaks including C-Si (283.9 eV), C=C (284.4 eV), C-C (284.9 eV), C-OH/C-O-Si (285.6 eV), C-O (286.5 eV), C=O (287.2 eV), and C(O)O (288.6 eV). The O 1s peak is divided into six Gaussian-Lorentzian peaks of O=C=O (530.2 eV), Ti-O (529.4 eV), C=O (531.2 eV), Si-O-Ti (532.7 eV), C-O (532.1 eV), and C-OH (534.1 eV). The N 1s spectrum is fitted in N-H (399.4 eV) and N-C (400.9 eV). Additionally, the Si 2p is separated into Si-C and Si-O-Ti whose binding energy is 101.8 eV and 102.5 eV, respectively. The Ti 2p is including Ti-O-Ti/Ti-O-Si at 458.8 eV and 464.5 eV [30]. The existence of Si-O-Ti, N-C, C-Si, N-H, and Ti-O-Ti peaks suggest that GO is modified with nano- TiO_2 by IPTMS.

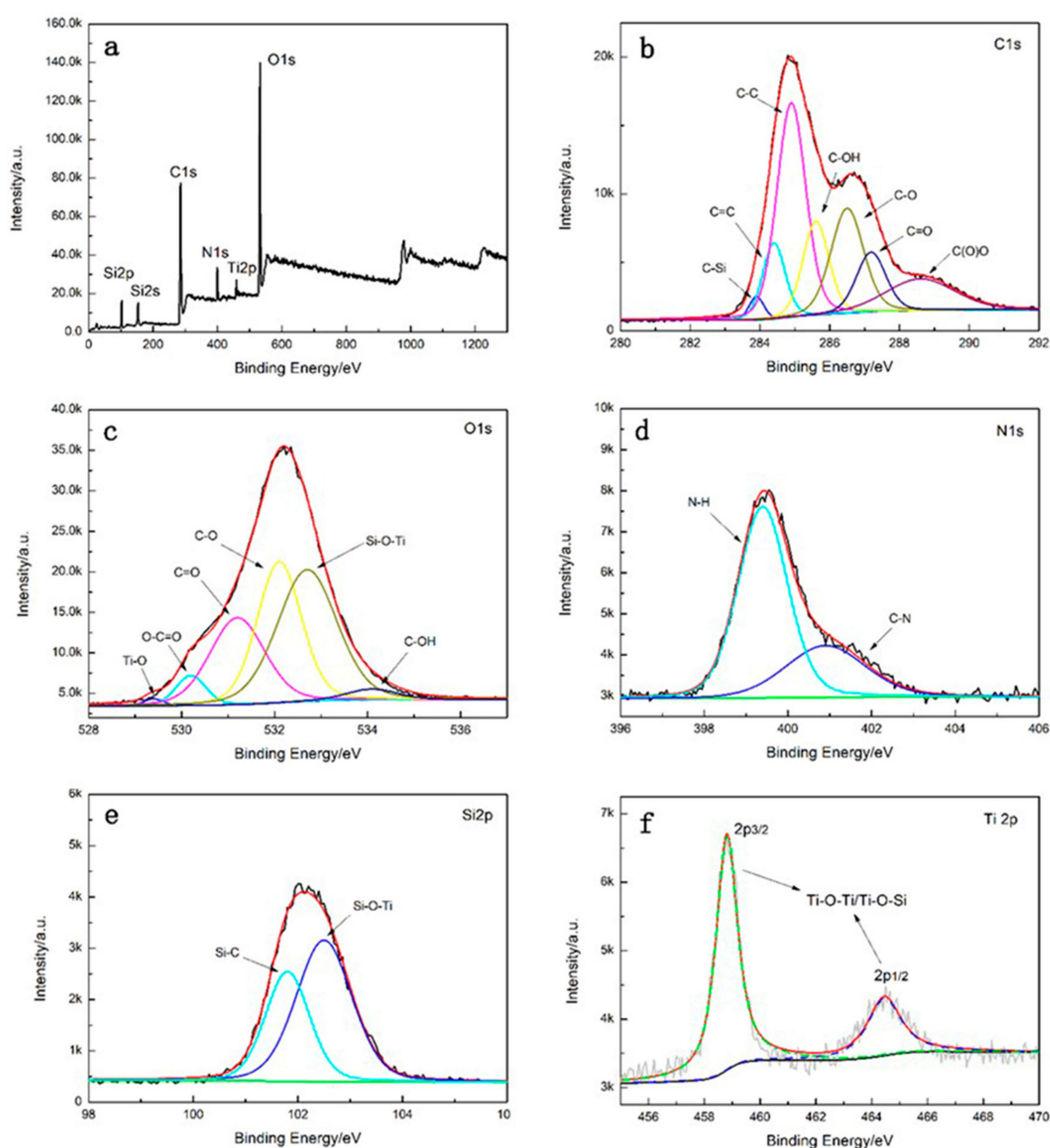


Figure 4. XPS survey spectra (a) and high resolution of spectra of (b) C1s, (c) O1s, (d) N1s, (e) Si2p, and (f) Ti2p of $\text{TiO}_2\text{-GO}$.

3.4. SEM Morphology

Figure 5 describes the morphology of GO and TiO₂-GO. Under this method, we can visualize the existence of nano-TiO₂ on the GO. The particle size distribution of Figure 5b₁ is shown in Figure 5c. It could be calculated that the average diameter of the nano-TiO₂ is about 160 nm. By comparison of Figure 5a₁,a₂,b₁,b₂, it is evident that TiO₂-GO turns to be unfolded and loose after the modification. This phenomenon is consistent with the result of XRD that the D-spacing is indeed increasing. However, the pristine GO seems to be aggregated to a certain degree. It may be related to the way of ordinary drying rather than the freeze-drying. Both of them show the characteristic wavy wrinkles on their surface. It could prove that our preparation and modification are successful and the observation of nano-TiO₂ on the GO surface would also illustrate their connection is by covalent bonds rather than the physical deposition.

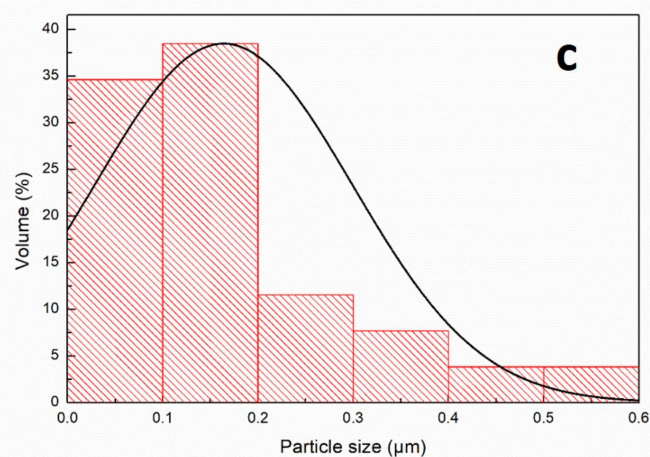
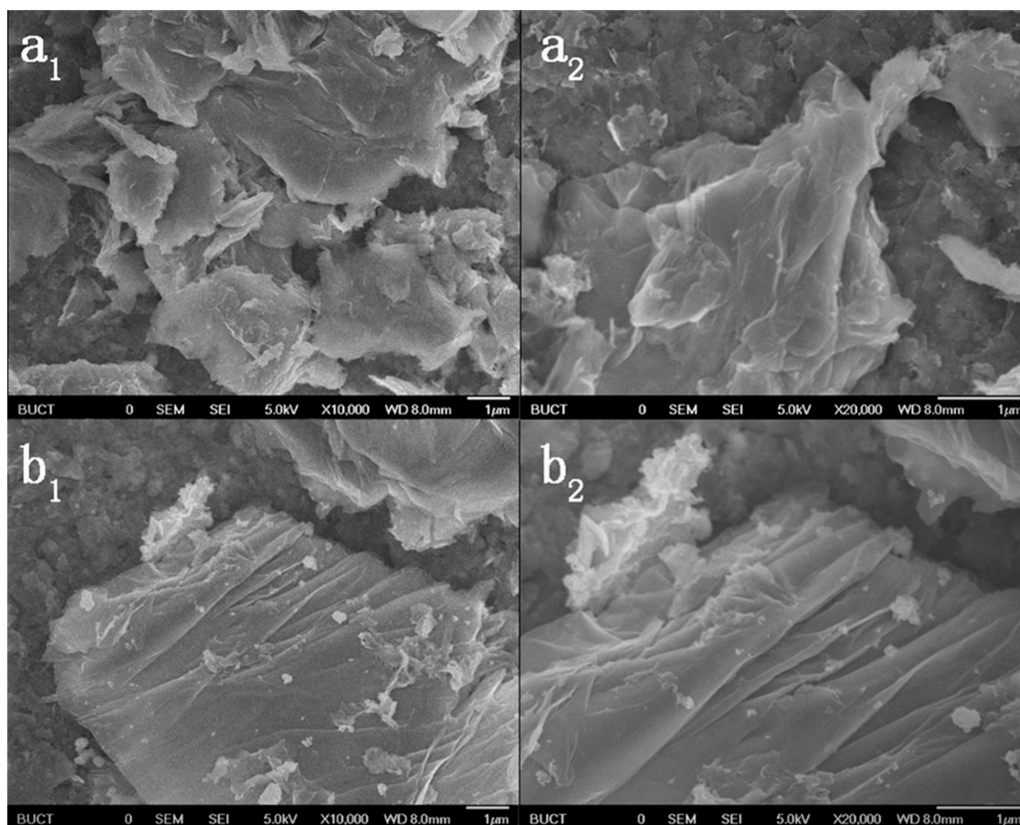


Figure 5. SEM image (a₁,a₂) GO, (b₁,b₂) TiO₂-GO, and (c) The particle size distribution of b₁.

3.5. TG Analysis

Figure 6 shows more details about the TGA thermograms of GO and TiO₂-GO. From starting temperature to 120 °C, TiO₂-GO suffered a small weight loss (12 wt.%). That is on account of the evaporation of the crystal water that forms in the process of synthesis [41]. At around 220 °C, the remained oxygen functional groups began to disintegrate which led to another loss (25 wt.%). The same phenomenon also occurs for GO. However, its mass loss is nearly 35 wt.%, which is much more than TiO₂-GO. That is attributed to the more account of the functional groups on the surface of GO. At a higher temperature region, GO's framework would be decomposed [42]. As a sort of inorganic particle, TiO₂ has excellent heat resistance with a high melting-point. Therefore, TiO₂-GO exhibits better thermal stability comparing to GO. The total mass loss is about 37 wt.% for TiO₂-GO and 49 wt.% for GO. That further demonstrates the existence of nano-TiO₂.

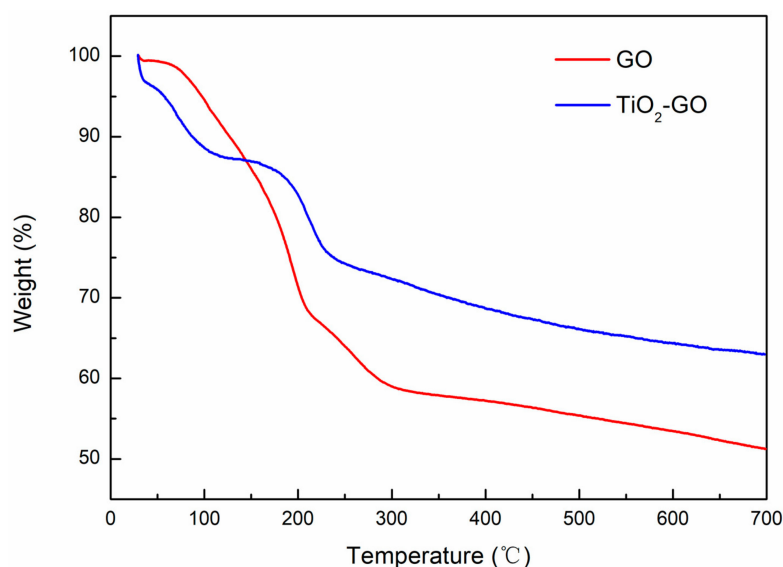


Figure 6. TGA curves of TiO₂-GO and GO.

3.6. Dispersion Test

Figure 7 exhibits the dispersity of GO and TiO₂-GO in water and ethanol at a concentration of 1 mg/mL. After sonification, the color of the two systems are a little different. The GO solution is dark brown, nearly black, while the TiO₂-GO is gray-black. After the modification, the character of TiO₂-GO changed from hydrophilic to hydrophobic. It precipitated in the water while GO remained well-dispersed after 3 h. However, TiO₂-GO could be homogeneous in ethanol while GO could not maintain a stable state. That mainly attributes to the hydrophilic group -OH and -COOH react with IPTMS and decorated with nano-TiO₂ at last. Both the nano-TiO₂ and remaining epoxide groups are hydrophobic, so it could significantly improve its compatibility with the organic solvent.

3.7. The Morphology of Epoxy Coatings

Figure 8 displays the morphologies of TiO₂-GO/EP and GO/EP. It reveals the state of TiO₂-GO and GO in EP. By contrast, with the help of IPTMS and nano-TiO₂, TiO₂-GO distributes more evenly in epoxy. From the high resolution of Figure 8a₂, severe agglomeration of GO can be seen in the matrix. However, the agglomeration of TiO₂-GO is much slighter. That is primarily ascribed to the difference of characteristics that TiO₂-GO is hydrophobic while GO is hydrophilic. Figure 8b₂ is a little vague due to the epoxy completely encapsulates the TiO₂-GO and the dielectric characteristic of it. That could be further verified that the TiO₂-GO possesses better compatibility with the epoxy, which is in accord with the above result.

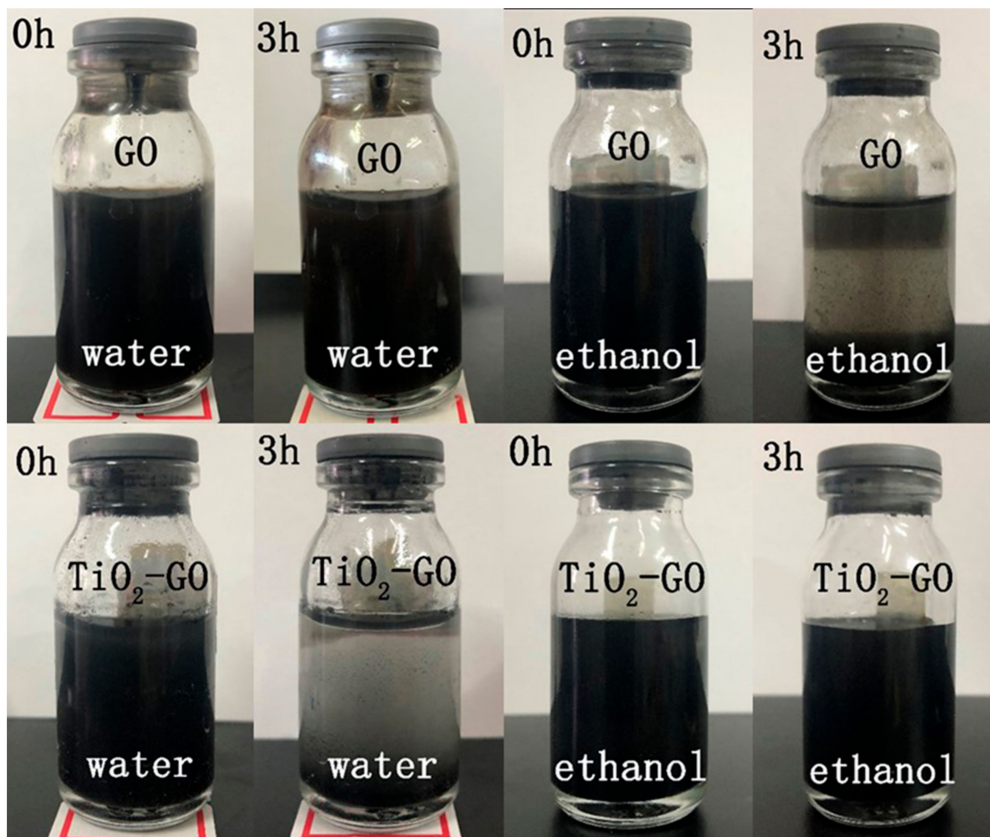


Figure 7. The comparison of TiO₂-GO and GO suspension in water and ethanol after setting for 1 h and 3 h.

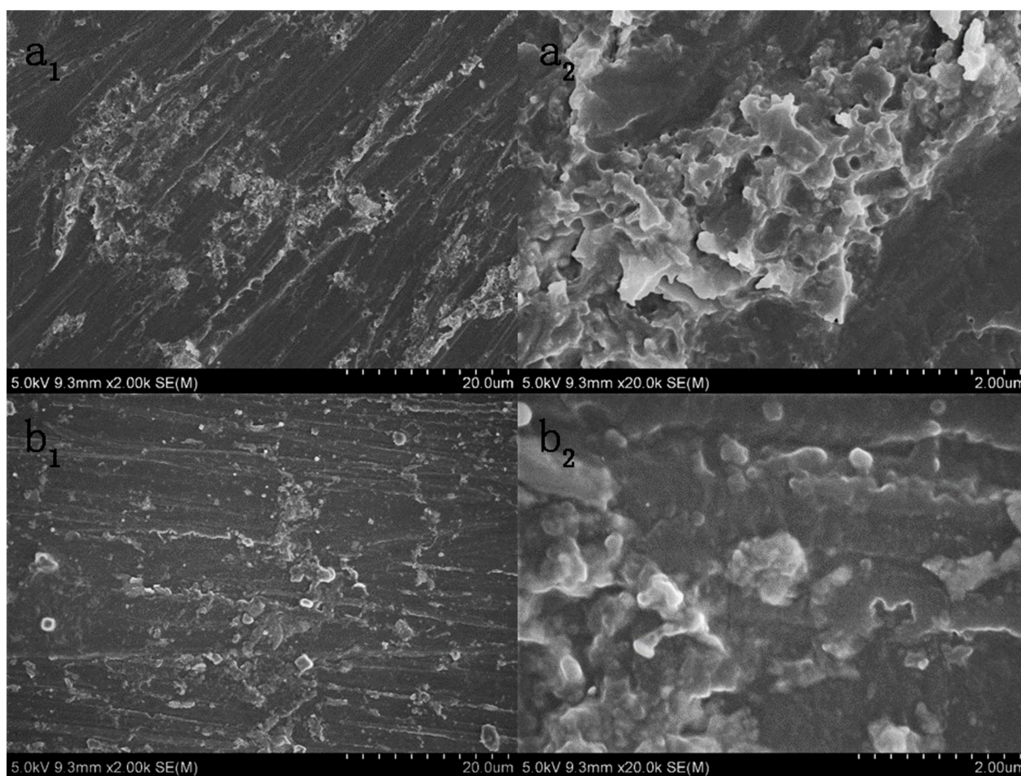


Figure 8. The morphologies of GO/EP (a₁,a₂) and TiO₂-GO/EP (b₁,b₂).

3.8. EIS Measurement

For coated substrates, the process of corrosion happens in three steps: (1) the coated substrate fully contacts with the corrosive medium while it is not penetrated, (2) the corrosive medium diffuses in coating through the defects while not reaching the substrate, and (3) the corrosive medium reaches the metal surface and results in damage [27]. For better evaluation of its corrosion behavior, the EP, GO/EP, TiO₂/EP, and TiO₂-GO/EP was explored by EIS. This could be seen from Figure 9a₁,b₁, all samples display a semicircle shape in Nyquist diagrams while the diameter of TiO₂-GO/EP is the largest among them. In general, the larger semicircle diameter is related to the lower corrosion rate [43]. Therefore, it means the corrosion rate of TiO₂-GO/EP is the lowest. As the test proceeded, the result was also proved. The EP, GO/EP, and TiO₂/EP appeared another semicircle after immersed 120 h which illustrated the electrolyte has penetrated in the coating while the film of TiO₂-GO/EP is still in the stage of only one semicircle. That means TiO₂-GO plays an important role in epoxy for anti-corrosion, it distributes uniform in the system that making the film much denser to impede the electrolyte effectively.

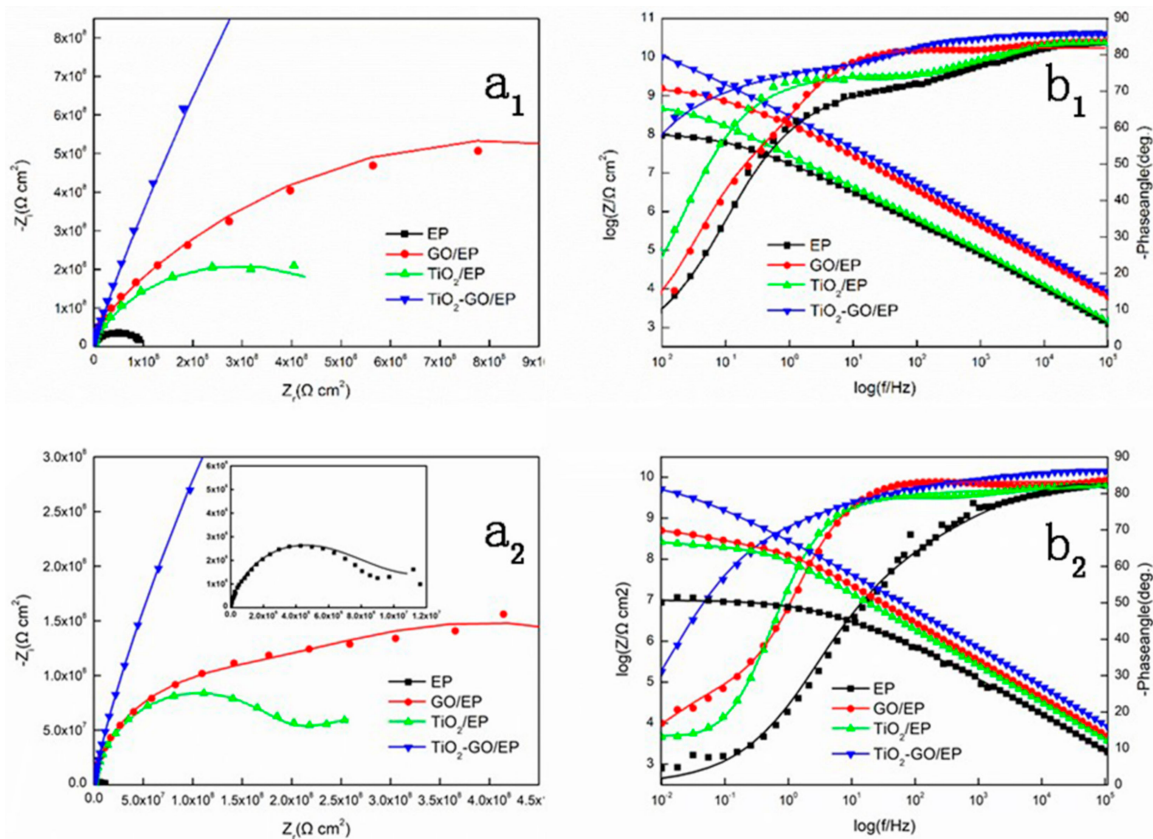


Figure 9. Nyquist(a₁) and Bode(b₁) spectrum after immersing 1 h; Nyquist(a₂) and Bode(b₂) spectrum after immersing 120 h.

Figure 9a₂,b₂ is the bode plots of four samples in different stages. The value of Z at low frequency ($|Z|_{0.01 \text{ Hz}}$) is a measure of corrosion resistance and higher $|Z|_{0.01 \text{ Hz}}$ indicates a better corrosion resistant coating on the metal substrate [44]. All the films show a decent performance at the initiative phase especial the systems with nano-fillers. Furthermore, among three sorts of powders, the positive effect of TiO₂-GO is the most significant; its value of $|Z|_{0.01 \text{ Hz}}$ reached $10^{10} \Omega \text{ cm}^2$ which was larger than the others. After immersion for about 120 h, all the film performance declined to varying degrees. The degradation of EP and GO/EP are more serious, especially the EP film, which is down by an order of magnitude from $10^8 \Omega \text{ cm}^2$ to about $10^7 \Omega \text{ cm}^2$. While the decline of nano-TiO₂/EP and TiO₂-GO/EP is not significant at the same time. That is primarily attributed to the excellent dispersity

of the nano-filler. Therefore, it lays down in matrix homogeneously and forms a zigzag structure that extends the permeation distance of electrolyte. The change of phase angle of four samples could also reflect the barrier result. Only one relaxation time could be seen of all the films at the beginning stage. However, with the increment of the immersion time, all the samples appear two relaxation times except the TiO₂-GO/EP, and its phase angle remains the largest, which is about -85° . That would illustrate the positive effects of nano-fillers on the film and the TiO₂-GO/EP possesses the best anti-corrosion property.

For better interpret the EIS data, the results are fitted by electrical circuit (Figure 10). The R_s , R_{cr} , R_{ct} , CPE_c , and CPE_{dl} represent the solution resistance, coating resistance, charge transfer resistance, and constant phase element of the coating and double layer, respectively. To model the electrochemical behavior of the system, a constant phase element associated with an exponent ($0 \leq n \leq 1$) was used to replace the capacitor for representing the experimental deviation from the semi-circle capacitance behavior since the heterogeneity of the coating surface [45]. The CPE could consider as a real resistance when $n = 0$ and a completely capacitance when $n = 1$. The fitting rules were as follows: The Nyquist diagram of the samples, which is one semicircle, was fitted by Figure 10a. In this period, a small amount of electrolyte has diffused in the coating which leads to the R_{cr} decreases with the immersion time increases. Therefore, the R_{ct} is no longer considered infinite, that could not be ignored in fitting process. The rest with two semicircle samples were fitted by Figure 10b. At this stage, the electrolyte reaches the substrates and reacts with it. That results in the lower value of R_{ct} which need to be fitted in parallel with CPE_{dl} . The electrochemical parameters after fitting are shown in Table 1.

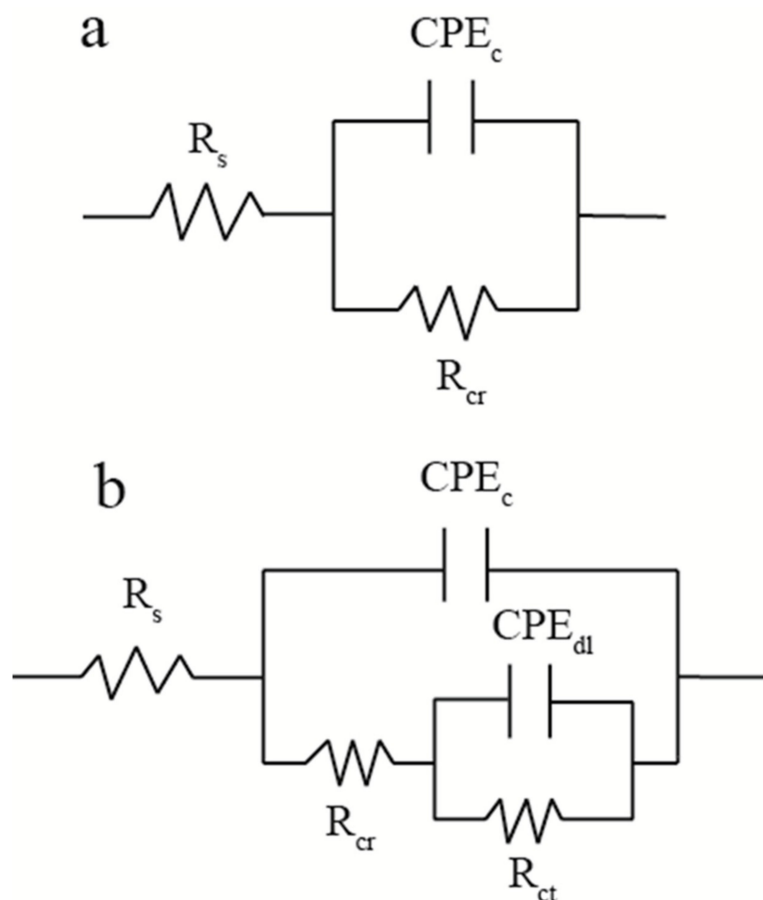


Figure 10. The equivalent electrical circuit used for fitting EIS data (a,b).

Table 1. The electrochemical parameters after fitting of all samples immersed in 3.5% NaCl solution for 1 and 120 h.

Sample	Time/h	$R_s(\Omega \text{ cm}^2)$	Q_c		$R_{ct}(\Omega \text{ cm}^2)$	Q_{dl}		$R_{ct}(\Omega \text{ cm}^2)$
			$Y_0(\Omega^{-1} \text{ cm}^{-2} \text{ s}^n)$	n		$Y_0(\Omega^{-1} \text{ cm}^{-2} \text{ s}^n)$	n	
EP	1 h	0.01	6.766×10^{-8}	0.8895	5.64×10^7			
GO/EP	1 h	0.01	9.365×10^{-9}	0.894	1.173×10^9			
TiO ₂ /EP	1 h	0.01	5.854×10^{-9}	0.8639	4.939×10^9			
TiO ₂ -GO/EP	1 h	0.01	5.869×10^{-10}	0.9014	1.501×10^{10}			
EP	120 h	0.01	2.702×10^{-9}	0.9102	9.947×10^5	2.572×10^{-11}	0.4752	1.098×10^7
GO/EP	120 h	0.01	3.119×10^{-9}	0.9243	7.939×10^8	4.92×10^{-9}	0.7169	5.988×10^8
TiO ₂ /EP	120 h	0.01	9.607×10^{-9}	0.9218	1.625×10^8	6.08×10^{-9}	0.5517	5.44×10^8
TiO ₂ -GO/EP	120 h	0.01094	6.24×10^{-10}	0.8986	5.149×10^9			

4. Conclusions

In this paper, we put forward a novel technique method to decorate GO with nano-TiO₂ by using IPTMS. One of the advantages of IPTMS, comparing to the regular silane coupling agent like KH550 or KH560, is that it could react with all the hydrophilic groups of GO (–OH and –COOH) and preserve the hydrophobic group (–CH(O)CH–). Therefore, after the modification, TiO₂–GO would possess better compatibility with epoxy in theory, which is a crucial factor in improving the performance. Through the characterization results, it can be obtained that with the help of IPTMS nano-TiO₂ successfully combined with GO through chemical bonds, and it indeed exhibits the good dispersity in the solvent system. In the meantime, the TiO₂–GO/EP shows the outstanding anti-corrosion property from the EIS test. The results confirm that according to our modification methods, the combination of GO and nano-TiO₂ could achieve the effect that one plus one is greater than two. Furthermore, these methods could be not only applied in this field, but also the other relevant area.

Author Contributions: Data curation, W.L.; Formal analysis, B.S.; Funding acquisition, Y.S.; Investigation, W.L. and S.Z.; Project administration, Y.S.; Resources, W.L., F.Z. and C.L.; Software, N.Z.; Supervision, Y.S. and H.Y.; Writing – original draft, B.S. All authors have read and agreed to the published version of the manuscript.

Funding: This research was supported by Key Research & Development Program of Shandong Province (grant number, 2019JZZY010355).

Acknowledgments: The authors appreciate Beijing University of Chemical Technology for EIS and SEM measurements.

Conflicts of Interest: The authors declare no conflict of interest.

References

1. Tang, Z.L. Corrosion science general-purpose data model and interface (II): OOD design and corrosion data markup language (CDML). *Sci. China Ser. E Technol. Sci.* **2008**, *51*, 1850–1857. [\[CrossRef\]](#)
2. Gong, L.X.; Zhao, L.; Tang, L.C.; Liu, H.Y.; Mai, Y.W. Balanced electrical, thermal and mechanical properties of epoxy composites filled with chemically reduced graphene oxide and rubber nanoparticles. *Compos. Sci. Technol.* **2015**, *121*, 104–114. [\[CrossRef\]](#)
3. Vaisakh, S.S.; Mahesh, K.V.; Balanand, S.; Metz, R.; Hassanzadeh, M.; Ananthakumar, S. MAX phase ternary carbide derived 2-D ceramic nanostructures [CDCN] as chemically interactive functional fillers for damage tolerant epoxy polymer nanocomposites. *RSC Adv.* **2015**, *5*, 16521–16531. [\[CrossRef\]](#)
4. Majd, M.T.; Shahrabi, T.; Ramezanzadeh, B. The role of neodymium based thin film on the epoxy/steel interfacial adhesion and corrosion protection promotion. *Appl. Surf. Sci.* **2019**, *464*, 516–533. [\[CrossRef\]](#)
5. Zhang, H.; Wang, L.B.; Zhou, A.G.; Shen, C.J.; Dai, Y.H.; Liu, F.F.; Chen, J.F.; Li, P.; Hu, Q.K. Effects of 2-D transition metal carbide Ti₂CT_x on properties of epoxy composites. *RSC Adv.* **2016**, *6*, 87341–87352. [\[CrossRef\]](#)
6. Ramezanzadeh, B.; Moghadam, M.H.M.; Shohani, N.; Mandavian, M. Effects of highly crystalline and conductive polyaniline/graphene oxide composites on the corrosion protection performance of a zinc-rich epoxy coating. *Chem. Eng. J.* **2017**, *320*, 363–375. [\[CrossRef\]](#)

7. Ye, Y.W.; Zhang, D.W.; Liu, T.; Liu, Z.Y.; Liu, W.; Pu, J.B.; Chen, H.; Zhao, H.C.; Li, X.G. Improvement of anticorrosion ability of epoxy matrix in simulate marine environment by filled with superhydrophobic POSS-GO nanosheets. *J. Hazard. Mater.* **2019**, *364*, 244–255. [[CrossRef](#)]
8. Wang, T.; Ge, H.Y.; Zhang, K.L. A novel core-shell silica@graphene straticulate structured antistatic anticorrosion composite coating. *J. Alloy. Compd.* **2018**, *745*, 705–715. [[CrossRef](#)]
9. Zaman, I.; Phan, T.T.; Kuan, H.C.; Meng, Q.S.; La, L.T.B.; Luong, L.; Yousf, O.; Ma, J. Epoxy/graphene platelets nanocomposites with two levels of interface strength. *Polymer* **2011**, *52*, 1603–1611. [[CrossRef](#)]
10. Chen, L.; Chai, S.G.; Liu, K.; Ning, N.Y.; Gao, J.; Liu, Q.F.; Chen, F.; Fu, Q. Enhanced epoxy/silica composites mechanical properties by introducing graphene oxide to the interface. *ACS Appl. Mater. Interfaces* **2012**, *4*, 4398–4404. [[CrossRef](#)]
11. Liu, Y.W.; Chen, Y. Anticorrosion performance of epoxy-resin coating incorporating talcum powder loaded with sodium tungstate. *Int. J. Electrochem. Sci.* **2018**, *13*, 530–541. [[CrossRef](#)]
12. Ahmed, N.M.; El-Gawad, W.M.A.; Souaya, E.R. Study on the corrosion protection performance of new ferrite/kaolin core-shell pigments in epoxy-based paints. *Anti-Corros. Methods Mater.* **2016**, *63*, 36–46. [[CrossRef](#)]
13. Wan, Y.J.; Tang, L.C.; Gong, L.X.; Yan, D.; Li, Y.B.; Wu, L.B.; Jiang, J.X.; Lai, G.Q. Grafting of epoxy chains onto graphene oxide for epoxy composites with improved mechanical and thermal properties. *Carbon* **2014**, *69*, 467–480. [[CrossRef](#)]
14. Li, G.; Cui, H.Y.; Zhou, J.C.; Hu, W.J. Improvements of nano-TiO₂ on the long-term chloride resistance of concrete with polymer coatings. *Coatings* **2019**, *9*, 323. [[CrossRef](#)]
15. Ma, Y.; Di, H.H.; Yu, Z.X.; Liang, L.; Lv, L.; Pan, Y.; Zhang, Y.Y.; Yin, D. Fabrication of silica-decorated graphene oxide nanohybrids and the properties of composite epoxy coatings research. *Appl. Surf. Sci.* **2016**, *360*, 936–945. [[CrossRef](#)]
16. Palraj, S.; Selvaraj, M.; Maruthan, K.; Rajagopal, G. Corrosion and wear resistance behavior of nano-silica epoxy composite coatings. *Prog. Org. Coat.* **2015**, *81*, 132–139. [[CrossRef](#)]
17. Ramezanzadeh, B.; Attar, M.M. Studying the effects of micro and nano sized ZnO particles on the corrosion resistance and deterioration behavior of an epoxy-polyamide coating on hot-dip galvanized steel. *Prog. Org. Coat.* **2011**, *71*, 314–328. [[CrossRef](#)]
18. Novoselov, K.S.; Geim, A.K.; Morozov, S.V.; Jiang, D.; Zhang, Y.; Dubonos, S.V.; Grigorieva, I.V.; Firsov, A.A. Electric field effect in atomically thin carbon films. *Science* **2004**, *306*, 666–669. [[CrossRef](#)]
19. Park, K.S.; Yi, K.S. Bipolar supercurrent, differential conductance and critical current in a nano transistor of a graphene-based junction. *J. Korean Phys. Soc.* **2007**, *50*, 1873–1877. [[CrossRef](#)]
20. Balandin, A.A.; Ghosh, S.; Bao, W.Z.; Calizo, I.; Teweldebrhan, D.; Miao, F.; Lau, C.N. Superior thermal conductivity of single-layer graphene. *Nano Lett.* **2008**, *8*, 902–907. [[CrossRef](#)]
21. Lee, C.; Wei, X.D.; Kysar, J.W.; Hone, J. Measurement of the elastic properties and intrinsic strength of monolayer graphene. *Science* **2008**, *321*, 385–388. [[CrossRef](#)] [[PubMed](#)]
22. Nair, R.R.; Blake, P.; Grigorenko, A.N.; Novoselov, K.S.; Booth, T.J.; Stauber, T.; Peres, N.M.R.; Geim, A.K. Fine structure constant defines visual transparency of graphene. *Science* **2008**, *320*, 1308. [[CrossRef](#)] [[PubMed](#)]
23. Lu, G.H.; Ocola, L.E.; Chen, J.H. Reduced graphene oxide for room-temperature gas sensors. *Nanotechnology* **2009**, *20*, 445502. [[CrossRef](#)] [[PubMed](#)]
24. Chen, C.; Cai, W.M.; Long, M.C.; Zhou, B.X.; Wu, Y.H.; Wu, D.Y.; Feng, Y.J. Synthesis of Visible-Light Responsive Graphene Oxide/TiO₂ Composites with p/n Heterojunction. *ACS Nano* **2010**, *4*, 6425–6432. [[CrossRef](#)] [[PubMed](#)]
25. Wu, Z.S.; Zhou, G.M.; Yin, L.C.; Ren, W.; Li, F.; Cheng, H.M. Graphene/metal oxide composite electrode materials for energy storage. *Nano Energy* **2012**, *1*, 107–131. [[CrossRef](#)]
26. Lin, Y.T.; Don, T.M.; Wong, C.J.; Meng, F.C.; Lin, Y.J.; Lee, S.Y.; Lee, C.F.; Chiu, W.Y. Improvement of mechanical properties and anticorrosion performance of epoxy coatings by the introduction of polyaniline/graphene composite. *Surf. Coat. Technol.* **2019**, *374*, 1128–1138. [[CrossRef](#)]
27. Pourhashem, S.; Vaezi, M.R.; Rashidi, A.; Bagherzadeh, M.R. Distinctive roles of silane coupling agents on the corrosion inhibition performance of graphene oxide in epoxy coatings. *Prog. Org. Coat.* **2017**, *111*, 47–56. [[CrossRef](#)]
28. Wan, Y.J.; Gong, L.X.; Tang, L.C.; Wu, L.B.; Jiang, J.X. Mechanical properties of epoxy composites filled with silane-functionalized graphene oxide. *Compos. Part A Appl. Sci. Manuf.* **2014**, *64*, 79–89. [[CrossRef](#)]

29. Yu, Z.X.; Di, H.H.; Ma, Y.; He, Y.; Liang, L.; Lv, L.; Ran, X.; Pan, Y.; Luo, Z. Preparation of graphene oxide modified by titanium dioxide to enhance the anti-corrosion performance of epoxy coatings. *Surf. Coat. Technol.* **2015**, *276*, 471–478. [CrossRef]
30. Liu, J.H.; Yu, Q.; Yu, M.; Li, S.M.; Zhao, K.; Xue, B.; Zu, H. Silane modification of titanium dioxide-decorated graphene oxide nanocomposite for enhancing anticorrosion performance of epoxy coatings on AA-2024. *J. Alloy. Compd.* **2018**, *744*, 728–739. [CrossRef]
31. Shi, H.W.; Liu, F.C.; Yang, L.H.; Han, E.H. Characterization of protective performance of epoxy reinforced with nanometer-sized TiO₂ and SiO₂. *Prog. Org. Coat.* **2008**, *62*, 359–368.
32. Duong, H.P.; Hung, C.H.; Dao, H.C.; Le, M.D.; Chen, C.Y. Modification of TiO₂ nanotubes with 3-aminopropyl triethoxysilane and its performances in nanocomposite coatings. *New J. Chem.* **2018**, *42*, 8745–8751.
33. Botas, C.; Alvarez, P.; Blanco, P.; Granda, M.; Blanco, C.; Santamaria, R.; Romasanta, L.J.; Verdejo, R.; Lopez-Manchado, M.A.; Menendez, R. Graphene materials with different structures prepared from the same graphite by the Hummers and Brodie methods. *Carbon* **2013**, *65*, 156–164.
34. Huang, N.M.; Lim, H.N.; Chia, C.H.; Yarmo, M.A.; Muhamad, M.R. Simple room-temperature preparation of high-yield large-area graphene oxide. *Int. J. Nanomed.* **2011**, *6*, 3443–3448.
35. Remyamol, T.; John, H.; Gopinath, P. Synthesis and nonlinear optical properties of reduced graphene oxide covalently functionalized with polyaniline. *Carbon* **2013**, *59*, 308–314.
36. Li, A.P.; Kan, C.Y.; Du, Y.; Liu, D.S. Study on the evolvement of structure in synthesis of urea-formaldehyde resins by FTIR. *Acta Phys. Chim. Sin.* **2006**, *22*, 873–877.
37. Parhizkar, N.; Ramezanzadeh, B.; Shahrabi, T. Corrosion protection and adhesion properties of the epoxy coating applied on the steel substrate pre-treated by a sol-gel based silane coating filled with amino and isocyanate silane functionalized graphene oxide nanosheets. *Appl. Surf. Sci.* **2018**, *439*, 45–59.
38. Parhizkar, N.; Shahrabi, T.; Ramezanzadeh, B. Synthesis and characterization of a unique isocyanate silane reduced graphene oxide nanosheets; screening the role of multifunctional nanosheets on the adhesion and corrosion protection performance of an amido-amine cured epoxy composite. *J. Taiwan Inst. Chem. Eng.* **2018**, *82*, 281–299.
39. Pourhashem, S.; Vaezi, M.R.; Rashidi, A. Investigating the effect of SiO₂-graphene oxide hybrid as inorganic nanofiller on corrosion protection properties of epoxy coatings. *Surf. Coat. Technol.* **2017**, *311*, 282–294.
40. Ramezanzadeh, B.; Ahmadi, A.; Mandavian, M. Enhancement of the corrosion protection performance and cathodic delamination resistance of epoxy coating through treatment of steel substrate by a novel nanometric sol-gel based silane composite film filled with functionalized graphene oxide nanosheets. *Corros. Sci.* **2016**, *109*, 182–205.
41. Park, S.; An, J.; Piner, R.D.; Jung, I.; Yang, D.; Velamakanni, A.; Nguyen, S.T.; Ruoff, R.S. Aqueous suspension and characterization of chemically modified graphene sheets. *Chem. Mater.* **2008**, *20*, 6592–6594. [CrossRef]
42. Yu, Y.-H.; Lin, Y.-Y.; Lin, C.-H.; Chan, C.-C.; Huang, Y.-C. High-performance polystyrene/graphene-based nanocomposites with excellent anti-corrosion properties. *Polym. Chem.* **2014**, *5*, 535–550.
43. Chang, K.C.; Ji, W.F.; Lai, M.C.; Hsiao, Y.R.; Hsu, C.H.; Chuang, T.L.; Wei, Y.; Yeh, J.M.; Liu, W.R. Correction: Synergistic effects of hydrophobicity and gas barrier properties on the anticorrosion property of PMMA nanocomposite coatings embedded with graphene nanosheets. *Polym. Chem.* **2014**, *5*, 1049–1056.
44. Sun, W.; Wang, L.; Wu, T.; Pan, Y.; Liu, G. Synthesis of low-electrical-conductivity graphene/pernigraniline composites and their application in corrosion protection. *Carbon* **2014**, *79*, 605–614.
45. Brusciotti, F.; Snihirova, D.V.; Xue, H.; Montemor, M.F.; Lamaka, S.V.; Ferreira, M.G.S. Hybrid epoxy-silane coatings for improved corrosion protection of Mg alloy. *Corros. Sci.* **2013**, *67*, 82–90.

